Title

Label-free imaging and analysis of the effects of lipolysis products on primary hepatocytes.

Journal

Journal of biophotonics, 4(6)

ISSN

1864-0648

Authors

Schie, Iwan W IW
Wu, Jian J
Weeks, Tyler T
et al.

Publication Date

2011-06-10

Journal of
www. biophotonics-journal.org
BIOPHOTONICS

WILEY-VCH

J. Biophotonics **4**, No. 6, 425–434 (2011) / **DOI** 10.1002/jbio.201000086

Journal of BIOPHOTONICS

FULL ARTICLE

Label-free imaging and analysis of the effects of lipolysis products on primary hepatocytes

Iwan W. Schie[1], *Jian Wu*[2], *Tyler Weeks*[1], *Mark A. Zern*[2], *John C. Rutledge*[3], *and Thomas Huser*[*,1,3]

[1] NSF Center for Biophotonics Science and Technology, University of California, Davis, Sacramento, CA 95817, USA
[2] Division of Gastroenterology & Hepatology, Department of Internal Medicine, University of California, Davis, Sacramento, CA 95817, USA
[3] Division of Endocrinology, Clinical Nutrition, and Vascular Medicine, Department of Internal Medicine, University of California, Davis, Sacramento, CA 95817, USA

Received 30 July 2010, revised 6 September 2010, accepted 6 September 2010
Published online 27 September 2010

Key words: non-alcoholic steatohepatitis (NASH), non-alcoholic fatty liver disease (NAFLD), coherent anti-Stokes Raman scattering (CARS), non-linear microscopy, Raman spectroscopy, lipolysis, triglyceride-rich lipoproteins

Abbreviations: non-alcoholic steatohepatitis – NASH; non-alcoholic fatty liver disease – NAFLD; coherent anti-Stokes Raman scattering – CARS; triglyceride-rich lipoprotein – TGRL; very low density lipoprotein – VLDL; lipoprotein lipase – LpL, 13-hydroxy-9,11-octadecadienoic acid – 13-HODE; tumor necrosis factor/Fas – TNF/Fas; methionine and choline-deficient diet – MCDD; reactive oxygen species – ROS.

The increased accumulation of intracellular lipid droplets within hepatocytes is a pathologic hallmark of liver injury of various etiologies, especially non-alcoholic steatohepatitis (NASH). The dynamics, subcellular origin, and chemical composition of lipid droplets under various pathophysiologic conditions, however, remain poorly understood. We used coherent Raman microscopy and spontaneous Raman spectroscopy to monitor and analyze the formation of lipid droplets in living primary rat hepatocytes exposed to triglyceride-rich lipoprotein (TGRL) lipolysis products. After exposure to the complex fatty acid mixture released during the lipolysis process for 30 minutes, new lipid droplets rapidly appeared within hepatocytes and increased in size and number over the total observation period of 205 minutes. Raman spectroscopic analysis of individual intracellular lipid droplets before and after exposure to lipolysis products reveals that the major components of these droplets are esterified unsaturated fatty acids. We find that the fatty acid unsaturation ratio increases with droplet size. Control experiments with defined fatty acid mixtures reveal the complexity of the cellular response to assault by combinations of lipids.

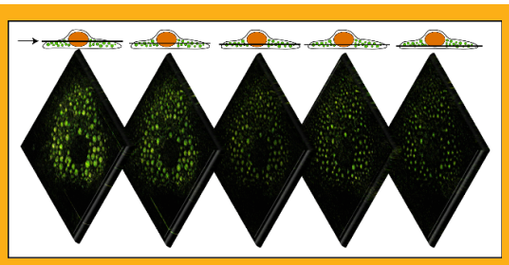

Optical sections at different heights through a lipid-filled rat hepatocyte obtained by CARS microscopy

* Corresponding author: e-mail: trhuser@ucdavis.edu

Journal of
BIOPHOTONICS

1. Introduction

The liver is a key organ for lipid metabolism and uptake, conversion, assembly, and export of lipoproteins are tightly regulated by hormones and lipokines (1). Fat accumulation (mainly in the form of triglycerides) in the liver occurs frequently, and can be harmless, reversible, and asymptomatic. On the other hand, the formation of lipid droplets may also represent a key first step for liver injury. Fatty liver disease in some non-alcoholic individuals, so-called non-alcoholic fatty liver diseases (NAFLD), including steatohepatitis (NASH), may be accompanied by fibrosis and progress to cirrhosis, which can develop into the end-stage of liver disease or hepatocellular carcinoma. However, after decades of exploration of the molecular mechanisms underlying the formation of lipid droplets in hepatocytes under various normal or pathologic conditions, the subcellular origins and chemical components, their impact on subcellular organelles, and the progression or pathological course of NAFLD and NASH remain poorly understood (2, 3). Moreover, recent evidence indicates that type rather than the amount of triglycerides in lipid droplets is critical in the sensitization of fatty liver to TNF/Fas-mediated steatohepatitis (4).

Various animal models of NASH are available, and they have provided significant insights into the mechanisms of NASH development (5–7). However, the utilization of isolated primary hepatocytes as a tool in NASH research allows dissecting the pathogenesis of lipid droplets, as well as their dynamic changes and impact on other cellular organelles at the molecular or subcellular levels in response to external stimuli (8).

Nonlinear microscopy techniques, such as second harmonic generation (SHG), provide a new approach to detecting and studying fibrotic liver tissue without the need for exogenous contrast agents, i.e. stains or fluorescent labels (9, 10). Unfortunately, SHG is only sensitive to the symmetry and organization of cellular structures and does not provide the chemical contrast necessary to specifically image lipids. Third harmonic generation has been used quite successfully to image lipid droplets, but it also lacks chemical specificity (11). Coherent anti-Stokes Raman scattering (CARS) microscopy is a relatively new approach allowing for chemical specificity based on intrinsic Raman-active molecular vibrations of the sample. By combining two short-pulsed near-infrared laser sources and overlaying them both spatially and temporally at the sample it is possible to coherently probe specific molecular vibrations with a spatial resolution on the sub-micron length scale. Due to the intensity dependence of the signal generation only molecules within the combined focal volume of both laser beams will generate a CARS signal providing confocal optical sample discrimination without the need for a confocal pinhole. By taking these advantages into consideration, CARS becomes particularly well-suited for the study of dynamic biological systems, such as living cells, where perturbations due to fluorescent stains could affect the outcome of an experiment (12–20).

CARS has recently been used to observe lipid droplets in steatotic tissue of a rat NASH model fed methionine and choline-deficient diet (MCDD) (14). However, no study which investigates the dynamic changes of lipid droplets in live primary hepatocytes with CARS has so far been performed. Here, we use CARS microscopy in a time-lapsed manner to monitor lipid accumulations in hepatocytes after exposure to lipolysis products derived from human triglyceride-rich lipoprotein (TGRL). We hypothesize that the complex fatty acid mixtures consisting of free fatty acids, phospholipids, monoglycerides, diglycerides and very low density lipoprotein (VLDL) remnant particles like low density lipoprotein (LDL) which are released from TGRL during lipolysis lead to the significantly higher lipotoxicity of TGRL lipolysis products. We also determined and compared the chemical composition of lipid droplets present in hepatocytes after exposure to lipolysis products using spontaneous Raman spectroscopy, which provides a full spectral assessment of the lipid droplet content. We find that new lipid droplets emerge primarily in the same cellular regions as naturally occurring droplets, but also, in new intracellular locations. Lipid droplets tend to fuse, but also continuously take up more fatty acids to form larger droplets under continuous exposure to lipolysis products. Raman-spectral analysis of the newly emerging lipid droplets reveals an increase in fatty acid bond unsaturation depending on the size of the lipid droplets. This study demonstrates that combining dynamic imaging through coherent anti-Stokes Raman microscopy with spontaneous Raman spectroscopy allows for a comprehensive chemical analysis of lipid droplet formation and composition in living hepatocytes. This approach enables us to characterize the response of hepatocytes to exposure to TGRL lipolysis products, a process that occurs continuously in the human body in the postprandial state. Imaging lipid metabolism in hepatocytes in response to high extracellular lipid concentration provides essential information of the effects of lipid fractions and their complex interplay on hepatocytes enabling a greater understanding of the pathogenesis of fatty liver diseases.

2. Materials and methods

2.1 Isolation and culture of primary rat hepatocytes

Sprague–Dawley rats (150–200 g) were purchased from Harlan Laboratory (Indianapolis, IN) and fed with a commercial diet and water. All animal experiments were performed according to the National Institutes of Health (NIH) guidelines for the ethical care and use of laboratory animals, and the experimental protocol was approved by the Institutional Animal Care and Use Committee (IACUC) of the University of California, Davis.

Primary hepatocytes were isolated from male Sprague–Dawley rats by a two-step collagenase perfusion procedure as described previously (21–23). Cell viability among different isolations, as assessed by exclusion of Trypan blue, was over 90%. Isolated hepatocytes were seeded on glass bottom culture dishes (MatTek Corporation, Ashland, MA) precoated with collagen type I from rat tail (Sigma, St. Louis, MO) at a density of 5×10^4 cells/cm^2, and incubated in William's medium E (Sigma-Aldrich Co. St. Louis, MO) containing 10% fetal bovine serum (FBS), insulin (0.02 unit/ml), 10 mM HEPES, 10 mM $NaHCO_3$ and antibiotics in an atmosphere of 5% CO_2 at 37 °C. 2 hours after seeding, the cells were washed with 0.01 M phosphate buffered saline (PBS) and medium was refreshed with the same supplements.

2.2 Isolation of triglyceride-rich lipoproteins from human blood

Male and female healthy human volunteers ages 18–55 were recruited from the University of California, Davis campus. The study was approved by the Human Subjects Research Committee of the University of California, Davis. The study aims and protocol were explained to each participant, and informed written consent was obtained. All studies were performed at the same time of day to eliminate any diurnal variables. Blood was drawn by venipuncture from subjects 3.5 hours following consumption of a moderately high fat meal into K_2-EDTA vacutainer tubes (BD – Becton, Dickinson and Company, Franklin Lakes, NJ) and centrifuged at 1,200 g for 10 minutes to obtain cell-free plasma. Plasma was treated with 0.01% sodium azide as a preservative and subjected to lipoprotein isolation as described previously (24), with minor modifications. Chylomicrons were removed from postprandial plasma by centrifuging for 30 minutes at 63,000 g prior to TGRL isolation. Lipid samples were dialyzed overnight at 4 °C in 0.9% NaCl and 0.01% EDTA and quantified for total triglyceride content using a kit (Sigma-Aldrich Co. St. Louis, MO). Lipolysis of TGRL was induced by the addition of bovine lipoprotein lipase (LpL), (Sigma-Aldrich, St. Louis, MO) at 3 Units/mL for 30 minutes at 37 °C, where indicated.

2.3 Treatment of primary hepatocytes with TGRL, LpL, and mixtures of fatty acids

After overnight culture, primary hepatocytes were washed with PBS, and medium was replaced with fresh complete medium. Fresh TGRL, isolated as described above, were directly added into the cell culture medium or mixed with LpL from bovine milk (Sigma, St. Louis, MO) in the complete William's E medium for 30 min, then added to the culture dishes. Palmitic acid (200 μMol) was first dissolved in ethanol, then transferred to water to create stock solutions and then added to the culture dishes to reach final concentrations as indicated. 13-HODE, (20 μMol), in ethanol was dried under nitrogen gas flow, and dissolved in medium before use. Hepatocytes were imaged immediately after exposure to TGRL or TGRL (50–100 mg/dL) + LpL (3 U/mL) using the CARS microscope. For spectral Raman analysis, primary hepatocytes were treated for 4 hours following the same protocols, fixed with 4% buffered paraformaldehyde, and washed with PBS.

2.4 CARS imaging of lipid droplet formation in primary rat hepatocytes

A 1064 nm Nd : YVO_4 laser (PicoTrain, HighQ Laser, Rankweil, Austria) with a 7 ps pulse width and a 76 MHz repetition rate is used as the Stokes pulse to generate the CARS signal and also serves as the pump laser for an Optical Parametric Oscillator (OPO, Levante, APE-Berlin, Berlin, Germany). The tunable OPO with a wavelength range between 790 nm–920 nm provides the pump pulse for the CARS signal generation with an average output power of 500 mW. Both beams are spatially and temporally overlapped and combined by a 970 nm dichroic mirror. To diminish possible photo damage to the cells, the laser repetition rate is reduced tenfold to 7.6 MHz by an electro-optical modulator (M350–160, Conoptics, Danbury, CT). The laser beams are then sent into an inverted optical microscope (IX71, Olympus America, Center Valley, PA) and focused to a diffraction-limited spot by a 60 ×-oil objective

Journal of
BIOPHOTONICS

(Olympus America, Center Valley, PA). The forward-directed CARS signal generated in the sample is separated from the laser beams by a dichroic mirror and a multiphoton short-pass filter (FF-01–750, Semrock, Rochester, NY) and is then collected by a single photon counting detector (APD, SPCM-AQR 14, Perkin-Elmer, Waltham, MA). The APD signal is processed using time-correlated single photon counting electronics (TimeHarp200, PicoQuant GmbH, Berlin, Germany) and displayed using image acquisition and analysis software (SymPhoTime, Pico Quant GmbH, Berlin, Germany).

To image lipid dynamics and lipid accumulation in primary rat hepatocytes after exposure to a combination of VLDL and LpL, the 1064 nm line of our $Nd:YVO_4$ laser was used as the Stokes probe beam. The OPO beam tuned to 816 nm, serves as the pump laser. Together, the two beams drive the strong aliphatic lipid CH_2 stretch vibration at 2854 cm^{-1} coherently, and generate a strong CARS signal at 661 nm, which was confirmed by detecting a narrowband CARS signal spectroscopically by an imaging spectrograph. All images were acquired at 256×256 pixels with an acquisition time of 1 min/image. To observe dynamic lipid accumulation, images were taken every 5 min over a total period of 4 hours. To maintain the samples at a constant temperature of 37 °C, the culture dishes were heated by an airstream incubator utilizing a feedback loop for temperature control. The cells were incubated with a mixture of 50–100 mg/dL TGRL and 3 units/ml LpL and placed on the inverted microscope immediately after treatment.

2.5 Spontaneous Raman analysis of single lipid droplets in hepatocytes

Spontaneous Raman spectra of single lipid droplets within hepatocytes were acquired on a custom-built inverted laser-tweezers Raman microscope. The main microscope platform consists of an Olympus IX-71 microscope equipped with a 100×, NA 1.4, oil immersion objective optimized for near-IR operation (Olympus America, Center Valley, PA). The laser source is an 80 mW, 785 nm diode-pumped solid-state laser (Crystalaser, Reno, NV). The spontaneously scattered Raman-shifted light is collected by the same microscope objective, dispersed by an imaging spectrograph (SP2300i, Roper Scientific, Trenton, NJ), equipped with a 300 lines/mm grating, and detected with a back-illuminated, thermoelectrically-cooled deep-depletion charge-coupled device (CCD) camera with 1340×100 pixels (PIXIS 100BR, Roper Scientific, Trenton, NJ) (25). To acquire spectra from individual lipid droplets the focal spot was positioned manually over the droplets within the hepatocytes. Background spectra were acquired from positions nearby, but outside the lipid droplets. Spectra were acquired for 30 s integration time for each droplet. Spectra were first processed by subtracting the individual background spectra. The resulting spectra were the further processed equally by subtracting a 5^{th} order polynomial to account for background fluorescence, smoothing by averaging 3 neighboring pixels, and normalized to the total area under the spectrum. To determine Raman peak ratios, peaks were fitted with a Lorentzian fit function and the amplitude values compared.

3. Results

3.1 Lipid accumulation after treatment with TGRL + LpL

To determine the dynamic response of hepatocytes to TGRL lipolysis products, primary rat hepatocytes were exposed to TGRL + LpL. Figure 1a shows rat hepatocytes imaged by CARS 1 min after the addition of TGRL lipolysis products. The other images shown in this figure were taken subsequently at the times indicated in each image. Here, the residual nonresonant background signal from four-wave mixing of the excitation lasers provides a phase-contrast like image of the cells in culture, enabling us to visualize their outlines and the characteristic two nuclei found in hepatocytes. Some lipid droplets with a diameter of 1 μm or less are visible in these cells based on their significantly higher resonant signal. In this series of images, to further enhance contrast for the lipid droplets, all images were processed equally by first intensity-thresholding the images until only the lipid droplets remained visible, then color-coding the lipid droplets and overlaying the images with the original. The number and size of the lipid droplets visible in Figure 1a are similar to those observed in untreated primary rat hepatocytes and occur as part of the natural cellular life cycle (26). Approximately 30 minutes after incubation with lipolysis products, new lipid droplets emerged, typically localized in the vicinity of existing lipid droplets. Also, a large number of small lipid droplets were found to develop throughout the cell's cytoplasm (Figure 1b–f). The majority of these new lipid droplets emerging in response to TGRL + LpL treatment were not as motile as those observed in untreated hepatocytes.

To confirm our findings from CARS microscopy, we also performed preliminary biochemical assays to determine cell stress and apoptosis after treatment of primary rat hepatocytes with lipolysis products. Cell stress was determined by measuring the release

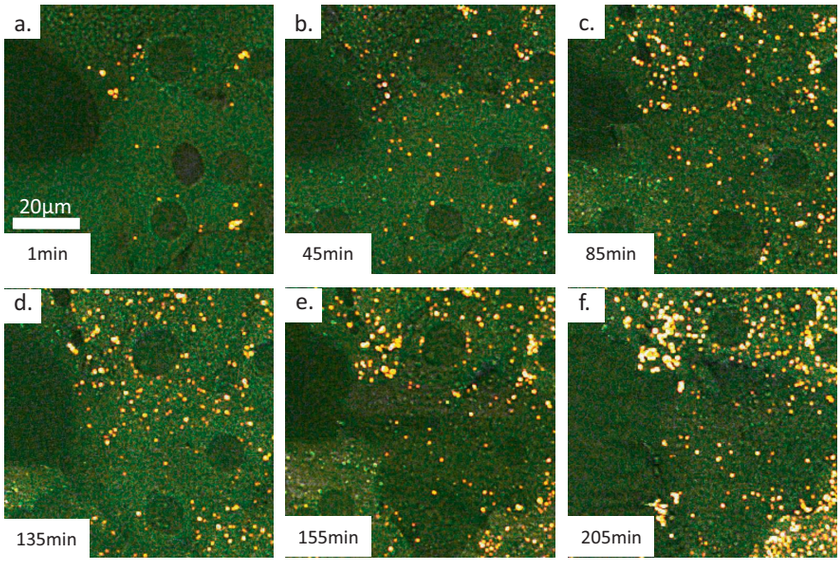

Figure 1 (online color at: www.biophotonics-journal.org) Time-lapse dynamic imaging of lipid droplet accumulations in primary rat hepatocytes after treatment with TGRL lipolysis products by CARS microscopy. Lipid droplets are shown in yellow false color as imaged by their 2845 cm^{-1} CH_2 vibrational mode, while contrast for the hepatocytes is mostly based on the nonresonant background signal. (**a**) 1 min; (**b**) 45 min; (**c**) 85 min; (**d**) 135 min; (**e**) 155 min; and (**f**) 205 min after the treatment.

of reactive oxygen species (ROS) from cells, while cell death was assessed using the Apoptag assay kit (Roche Pharmaceuticals, Basel, Switzerland). Hepatocytes were washed and plated (10,000 cells/well) on collagen-coated 96 well plates overnight. The next day cells were washed and then incubated with TGRL, TGRL lipolysis products, or individual fatty acids (palmitic acid (200 μM), oxidized linoleic acid (13-HODE, 20 μM), linoleic acid (100 μM), oleic acid (150 μM), or LPS (positive control; 10 μg/ml)) for 4 hours. To determine release of ROS, dihydroethidium (2 μM) was added to each well and the 0 hour measurements were taken immediately, followed by incubation of the cells at 37 °C in the dark. After 4 hours, additional measurements were taken and subtracted from the 0 h measurement. ROS release from untreated controls was compared with the 4 hour treatments with TGRL and TGRL lipolysis products. While neither the control cells, nor the TGRL-treated cells showed any noticeable sign of release of ROS, cells treated with TGRL lipolysis products exhibited a very significant increase in ROS generation. When testing for apoptosis induction, we found that the TGRL lipolysis product-treated cells displayed 2-fold higher and 13-HODE/LPS-treated cells 3-fold higher numbers of dead cells than the controls, where cell death typically ranked in the range of 5% of all cells.

3.2 Spectral analysis of cellular lipid accumulations

To analyze the effects of lipolysis product treatment on the composition of cellular lipid droplets, Raman spectra of lipid droplets were obtained over the spectral region from 500 to 3100 cm^{-1} from differently sized lipid droplets within hepatocytes. An average Raman spectrum obtained from 10 different droplets in an untreated control sample is shown in Figure 2a. This spectrum represents a typical lipid Raman spectrum composed mostly of contributions from C−C, C−H, and C−O bond vibrations (27–29).

Specifically, the 1266 cm^{-1} and 1302 cm^{-1} are an in-plane =C−H double bond vibration in cis conformation and a CH_2 twisting mode, respectively. The ratio between these two peaks can be used as an indicator for the degree of unsaturation in hydrocarbon chains. The 1446 cm^{-1} vibration is a combination of a CH_2 twisting mode and the 1455 cm^{-1} CH_2 scissoring mode and its intensity is a good measure of the total lipid content in the droplets. The peak at 1655 cm^{-1} is a C=C stretch vibration in the cis configuration, also representative of the degree of hydrocarbon chain unsaturation. The C=O ester group can be found at 1742 cm^{-1} and is indicative of triglyceride esterification within the lipid droplets. The broad 3000 cm^{-1} region which consists mostly of C−H stretching vibrations was excluded from the figure, because the peak response in the fingerprint region was more expressed and readily quantifiable because these peaks are well isolated compared to the rather crowded and convoluted high wavenumber region.

Previous studies (28, 30) showed that changes in the ν_{1655}/ν_{1446} and ν_{1266}/ν_{1302} peak ratios correlate well with the number of double bonds present in fatty acids and reflect the total degree of unsaturation. The peak ratio ν_{1655}/ν_{1446} of the lipid Raman spectrum for small lipid droplets (0.5 μm diameter) is 0.70 (see Figure 2a). According to Weng et al. (30)

Journal of
BIOPHOTONICS

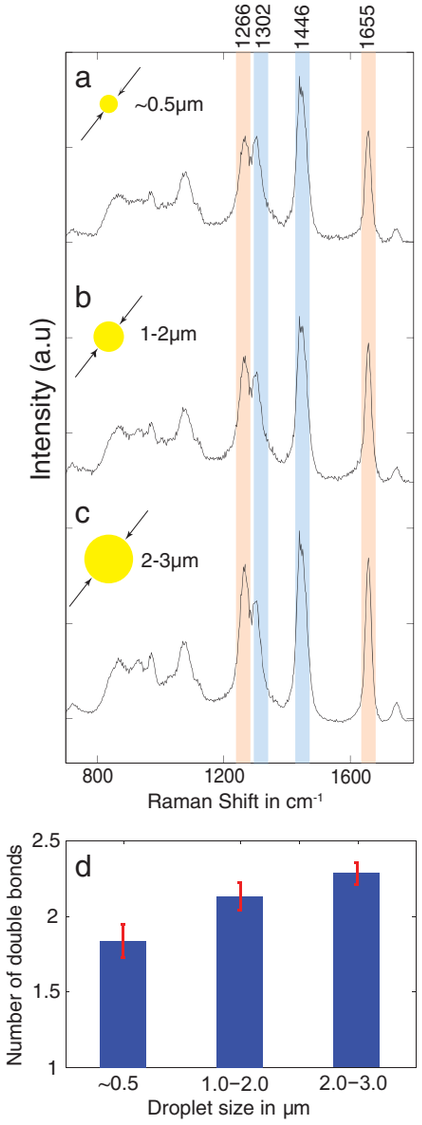

Figure 2 (online color at: www.biophotonics-journal.org) Spontaneous Raman spectra acquired from lipid droplets that have formed inside hepatocytes after incubation with TGRL lipolysis products for 2 hours. Each spectrum represents an average of spectra obtained from 10 individual droplets in the same size range. (**a**) Droplets with diffraction-limited diameter of 0.5 µm, (**b**) droplets with a diameter in the range from 1–2 µm, and (**c**) droplets with a diameter 2–3 µm. (**d**) The bar graph shows the average number and the standard deviation of C=C double bonds of all the droplets measured for the indicated droplet size. Note that the overall triglyceride content of the droplets appears to remain relatively unchanged as indicated by the intensity of the 1730 cm^{-1} peak, whereas the degree of unsaturation changes noticeably with size. The red framed peaks at 1266 cm^{-1} and 1655 cm^{-1} correspond to unsaturated chemical bonds whereas the blue framed peaks at 1302 cm^{-1} and at 1446 cm^{-1} correspond to saturated chemical bonds.

this ratio corresponds to an average number of 1.66 double bonds in a fatty acid, representing linoleic acid-like poly-unsaturation. Continuing with the criterion developed by Wang et al. (30), the ν_{1655}/ν_{1446} peak ratio for lipid droplets with a size of 1.0–2.0 µm in lipolysis product-treated cells corresponds to an increase in the average number of double bonds to 1.95 (see Figure 2b). This is complemented by another significant change in the ν_{1266}/ν_{1302} peak ratio, indicating that larger lipid droplets grow primarily through the addition of unsaturated fatty acids. An even higher level of unsaturation can be found in lipid droplets with an approximate size of 2.0–3.0 µm (Figure 2c), with an average of 2.11 unsaturated lipid bonds per fatty acid, indicating that even more unsaturated fatty acids are preferably accumulating in larger lipid droplets in TGRL lipolysis-product-treated cells. A statistical comparison of the average number of double bonds relative to the size of the lipid droplets is shown in the bar graph in Figure 2d.

To further investigate the effects of hepatic lipotoxicity using Raman spectroscopy and in an attempt to determine the response of cells to lipolysis product fractions, hepatocytes were also incubated with the saturated fatty acid palmitic acid, oxidized linoleic acid (13-HODE), or with a combination thereof. Figure 3a shows the averaged spectrum from lipid droplets in an untreated hepatocyte representing the control sample. Here, we have included the 3000 cm^{-1} CH-active region because significant changes were observed even in this high-wavenumber region. Fig 3b shows the average spectrum of hepatic lipid droplets generated in response to incubation with 13-HODE. This spectrum exhibits only subtle changes when compared with the control spectrum. In particular, interaction with 13-HODE leads to an increase in intensity of the 1655 cm^{-1} lipid peak, due to uptake of 13-HODE and its two unsaturated bonds. The observed increase in Raman peak intensities corresponds to an average of 2.10 unsaturated bonds per fatty acid within the cellular lipid droplet. Furthermore, we observe a broadening of the base of this peak which we attribute to spectral overlap with the hydroxyl group of 13-HODE.

Similarly, treatment with palmitic acid results in an increase in the 1302 cm^{-1} and the 1444 cm^{-1} peak (see Figure 3c). Both are representative of saturated lipid bonds, indicating that at least a fraction of palmitic acid is taken up by the cells and integrated into their lipid droplets. The average number of unsaturated bonds per fatty acid is 1.73 bonds, indicating that no major uptake of the saturated palmitic acid occurred. In contrast, treatment of hepatocytes with a combination of palmitic acid and 13-HODE leads to a stark change of the lipid droplet spectra (see Figure 3d). Here, the 860 cm^{-1} peak disappears and

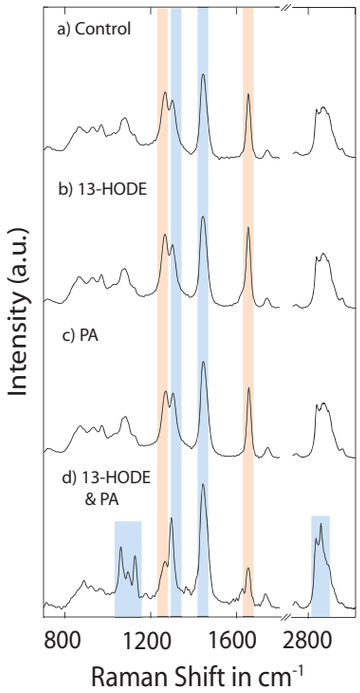

Figure 3 (online color at: www.biophotonics-journal.org) Spontaneous Raman spectra acquired over the entire Raman-active range from primary hepatocytes after exposure to different primary lipids for 2 hours. (**a**) Untreated control sample, (**b**) after incubation with the oxidized lipid 13-HODE, (**c**) after incubation with the saturated lipid palmitic acid, and (**d**) after incubation with a combination of 13-HODE and palmitic acid. The blue framed boxes indicate strong saturated peaks and the red framed boxes indicate unsaturated peaks.

a new peak at 891 cm^{-1} appears, corresponding to a CH_2 rocking vibration. The =C–H out of plane vibration at 969 cm^{-1} is still present. The previously broad peak between 1060 cm^{-1} and 1140 cm^{-1} has separated completely and now exhibits very sharp peaks at 1065 cm^{-1}, 1096 cm^{-1} and 1130 cm^{-1} corresponding to C–C stretch vibrations found in highly concentrated saturated fatty acids below the melting point. The 1266 cm^{-1} unsaturated lipid peak decreases, and large increases in the 1298 cm^{-1} and the 1444 cm^{-1} peaks indicate an overall higher degree of saturation in these lipid droplets corresponding to significant palmitic acid accumulation. Furthermore, a new peak at 1630 cm^{-1} corresponding to 13-HODE appears and the 1656 cm^{-1} unsaturated lipid peak also decreases significantly. The corresponding degree of unsaturation decreases dramatically to 0.76 bonds, the lowest value observed in this study. This decrease indicates that 13-HODE is a factor leading to the increased accumulation of saturated fatty acids in lipid droplets. Lastly, a strong increase in the Fermi resonance band near 2881 cm^{-1} can be observed, correlating well with the well-known spectrum of saturated lipids (29).

4. Discussion

In this study we demonstrate the application of time-lapse imaging of lipid droplet formation in living hepatocytes by coherent anti-Stokes Raman microscopy combined with the full biochemical compositional analysis gleaned from spontaneous Raman spectroscopy. We show that approximately 30 minutes after the incubation of hepatocytes with TGRL and LpL, TGRL lipolysis products generate new lipid droplets in close proximity to native lipid droplets. An analysis with spontaneous Raman spectroscopy of the newly formed lipid droplets generated in response to TGRL lipolysis product treatment revealed that the degree of fatty acid unsaturation increases in these new emerging droplets relative to the control sample. Furthermore, Raman spectral analysis of cells treated with a combination of 13-HODE and palmitic acid shows that palmitic acid is integrated into cellular lipid droplets at significant concentrations only in response to a combination of both fatty acids.

To determine the temporal response of hepatocytes to the exposure of TGRL lipolysis products, we also continuously imaged lipid accumulation in these cells using CARS microscopy. Lypolysis of TGRL by LpL yields free fatty acids, phospholipids, monoglycerides, diglycerides and VLDL remnant particles like IDL and LDL. This increased extracellular lipid concentration leads to a cellular influx of free fatty acids promoted by flip-flop movement across the plasma membrane or possibly by lipid transport proteins as shown in a number of recent studies (39, 40). Other mechanisms also contribute to an increased lipid uptake by cells. Approximately 30 minutes after exposure to lipolysis products, new lipid droplets emerge primarily in the vicinity of existing droplets. This indicates that lipid droplets are related to specific cellular compartments, such as the endoplasmic reticulum leaflets (26, 41–43).

To analyze the lipid composition of lipid droplets in treated cells, full Raman spectra of several lipid droplets in these cells were acquired and compared. Our results show that in hepatocytes treated with lipolysis products the concentration of unsaturated fatty acids in lipid droplets increases. As shown previously, the average number of unsaturated bonds in TGRL particles in blood plasma at 3h postprandially is 1.29 (29). Our measurement of lipid droplet composition inside hepatocytes, however, shows that the average number of unsaturated fatty acid bonds for small, newly emerging lipid droplets is 1.7. More-

over, the analysis of large lipid droplets (2.0–3.0 μm) inside hepatocytes shows that the average number of unsaturated fatty acid bonds is even higher at 2.1. This observation shows that new lipid droplets synthesized in hepatocytes during their exposure to TGRL lipolysis products contain significantly more unsaturated fatty acids than TGRLs themselves. A similar surprising observation was recently made by Corbin et al., (43) using magnetic resonance spectroscopy, who found that leptin-deficit obese (ob/ob) mice and methionine and choline-deficient diet (MCDD)-fed mice develop primarily triglyceride-rich lipid droplets with mono- and polyunsaturated fatty acids in their liver during the progression of fatty liver disease. The accumulation of unsaturated fatty acids in lipid droplets is attributed to an adapted cellular protection from lipotoxicity by triglyceride accumulation by Listenberger et al., (37). These authors observed that cells incubated with palmitic acid became more apoptotic than those treated with a combination of palmitic acid and oleic acid, which suggested that unsaturated fatty acids channel saturated fatty acid towards triglyceride lipid accumulation and help protect the cells from apoptosis.

To also study the effects of *oxidized* lipids, a significant byproduct of VLDL lipolysis, on lipid accumulation, we treated primary hepatocytes with palmitic acid, 13-HODE, and a combination of the two. Subsequently, the chemical composition of lipid droplets in these treated hepatocytes was analyzed by spontaneous Raman spectroscopy. The apparent morphology of these lipid droplets in terms of droplet size or the relative number of droplets was indistinguishable from those of untreated cells. Treatment with 13-HODE alone resulted in just minor changes in the Raman spectrum obtained from these cells, primarily a broadening of the 1655 cm^{-1} peak base and an increase in the intensity of this peak. This finding suggests that 13-HODE was taken up at least partially by the cell and incorporated into previously existing lipid droplets. Incubation of cells with palmitic acid alone also did not change the Raman spectra significantly; only slight increases in saturated lipids and overall lipid content as reflected by increased intensities of the 1302 cm^{-1} and the 1440 cm^{-1} peak were observed. On the other hand, treatment by the combination of palmitic acid and 13-HODE caused a very strong spectral response. Interestingly, the spectra obtained from cells treated in this way are remarkably reminiscent of those obtained from TGRL isolated from blood 8h after consumption of a moderately high fat meal (29). In particular, the occurrence of the sharp Raman peaks due to C–C skeletal modes in the 1050–1150 cm^{-1} range indicates the formation of a core of saturated fats where saturated lipids are tightly packed leading to strong interactions between adjacent lipid chains. The fact that we furthermore observe a strong increase in the 1730 cm^{-1} C=O peak would indicate that these lipids are also esterified, leading to highly saturated triglycerides. This, in turn leads to a highly lipotoxic environment likely causing the cell to synthesize even more unsaturated lipids to compensate for the accumulation of toxic saturated lipids.

5. Conclusions

CARS microscopy and Raman spectroscopy provide a new means of studying the effects of metabolic disorders and diseases, such as fatty liver disease, at the cellular level in living cells. We find that TGRL lipolysis caused rapid lipid droplet synthesis and accumulation in primary hepatocytes. Analysis of lipid droplet composition indicates that lipids in untreated cells are stored in the form of esterified triglycerides. Cells treated with lipolysis products rapidly synthesize new lipid droplets with a significantly higher degree of unsaturation, indicating that treated cells try to protect themselves against lipotoxicity by forming new lipid droplets. Further, cells treated with a mixture of palmitic acid and 13-HODE led to a significant integration of palmitic acid into lipid droplets leading to the formation of highly saturated lipid cores in these droplets.

Acknowledgements We would like to thank Dr. Ma Hnin-Hnin Aung in Rutledge's lab for collecting VLDL from volunteers, as well as the Dept. of Internal Medicine for intramural support. Dr. Rutledge was supported by NIH HL55667 and the Richard A. and Nora Eccles Harrison Endowed Chair in Diabetes Research. This work was supported in parts by the American Heart Association through the Grant-in-Aid program. Support by the National Institutes of Health, National Cancer Institute, under grant number 1U54CA136465-01 is acknowledged. This work was also supported in part by funding from the National Science Foundation. The Center for Biophotonics, an NSF Science and Technology Center, is managed by the University of California, Davis, under Cooperative Agreement No. PHY 0120999. Support is also acknowledged from the UCD Clinical Translational Science Center under grant number UL1 RR024146 from the National Center for Research Resources (NCRR). Part of this study was presented in the 60th Annual Meeting of the American Association for the Study of Liver Diseases (AASLD), Oct. 31–Nov. 3, 2009, Boston, MA.

Iwan W. Schie earned his Diploma in Biomedical Engineering from the Beuth University of Applied Science in Berlin, Germany, and is currently a Ph.D. candidate in the Department of Biomedical Engineering at the University of California, Davis, and the Center for Biophotonics Science and Technology. His major research interests are Raman spectroscopy and nonlinear microscopy, e.g. CARS, second harmonic generation and two-photon excited fluorescence and their applications to studying lipid related diseases.

Jian Wu is a Professor in the Department of Internal Medicine, Division of Gastroenterology & Hepatology, University of California, Davis Medical Center, in Sacramento, USA. Dr. Wu finished his medical education in 1983, and became a specialist in Gastroenterology & Hepatology in the Southeast University Medical College, Nanjing, China in 1988. He received his Ph.D. from the University of Umeå, Sweden. His research mainly focuses on the development of innovative drug, gene and cell therapy for liver diseases. His new research focus is on animal models of nonalcoholic steatohepatitis.

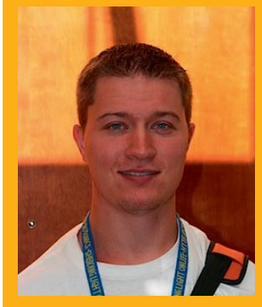

Tyler Weeks received his Ph.D. in Applied Science from the University of California, Davis. He obtained a B.S. degree in Physics from Brigham Young University in Provo, Utah. Until July 2010 he was a graduate student at the NSF Center for Biophotonics in Sacramento, USA, interested in nonlinear optics and label-free imaging. During this time, Tyler was a Scholar in the Lawrence Livermore National Laboratory Lawrence Scholarship Program. Since August 2010 he is a Process Engineer at Intel Portland Technology Development in Hillsboro, USA.

Mark A. Zern has been a researcher and active clinical hepatologist for more than 30 years. He is presently Professor of Internal Medicine, Fred and Pat Anderson Family Chair in Transplant Research, and Director, Transplant Research Program at the University of California, Davis Medical Center. Among other leadership roles, he has been the Chair of Gastroenterology and Hepatology at two institutions, of NIH-supported meetings an NIH study section, Chair of the Grants Review Committee of the American Liver Foundation, of the Liver Task Force of the Alpha-1 Foundation, and the founding President of the International Study Group for Stem Cell Therapy.

John C. Rutledge is a Professor in the Division of Cardiovascular Medicine and Co-Vice Chair for Research in the Department of Internal Medicine at the University of California Davis School of Medicine. He holds the Richard A. and Nora Eccles Harrison Endowed Chair for Diabetes Research.

Thomas Huser is an Associate Professor in the Department of Internal Medicine at the University of California, Davis. He also serves as Chief Scientist for the Center for Biophotonics Science and Technology, and Co-Director of the Translational Working Group for the Clinical Translational Science Center at UC Davis. Until 2005, Dr. Huser was a group leader for Biophotonics and Nanospectroscopy at Lawrence Livermore National Laboratory in Livermore, CA, where he developed and applied novel nano-biophotonics tools to characterize the nanosystems biology of individual cells. Dr. Huser obtained his Ph.D. in Physics from the University of Basel, Switzerland, where he worked primarily on near-field optical microscopy. At UC Davis he applies Raman spectroscopy and imaging, and single molecule fluorescence microscopy to biological and medical problems at the single cell level.

References

[1] F. Marra and C. Bertolani, Hepatology **50**, 957–969 (2009).
[2] C. L. Gentile and M. J. Pagliassotti, J. Nutr. Biochem. **19**, 567 (2008).
[3] J. K. Reddy and S. Rao, Am. J. Physiol. Gastrointest. Liver Physiol. **290**, G852 (2006).
[4] M. Marí, F. Caballero, A. Colell, A. Morales, J. Caballeria, A. Fernandez, C. Enrich, J. C. Fernandez-Checa, and C. García-Ruiz, Cell Metab. **4**, 185–198 (2006).
[5] J. C. Lo, Y. Wang, A. V. Tumanov, M. Bamji, Z. Yao, C. A. Reardon, G. S. Getz, and Y. X. Fu, Science **316**, 285 (2007).
[6] Q. Deng, H. She, J. H. Cheng, S. W. French, D. R. Koop, S. Xiong, and H. Tsukamoto, Hepatology **42**, 905–914 (2005).
[7] T. Ota, T. Takamura, S. Kurita, N. Matsuzawa, Y. Kita, M. Uno, H. Akahori, H. Misu, M. Sakurai, and Y. Zen, Gastroenterology **132**, 282–293 (2007).
[8] M. J. Gomez-Lechon, M. T. Donato, A. Martínez-Romero, N. Jiménez, J. V. Castell, and J. E. O'Connor, Chem. Biol. Interact. **165**, 106–116 (2007).
[9] P. J. Campagnola, M. Wei, A. Lewis, and L. M. Loew, Biophys. J. **77**, 3341–3349 (1999).
[10] W. Sun, S. Chang, D. C. S. Tai, N. Tan, G. Xiao, H. Tang, and H. Yu, J. Biomed. Opt. **13**, 064010 (2008).
[11] D. Débarre, W. Supatto, A. M. Pena, A. Fabre, T. Tordjmann, L. Combettes, M. C. Schanne-Klein, and E. Beaurepaire, Nat. Methods **3**, 47 (2006).
[12] I. W. Schie, T. Weeks, G. P. McNerney, S. Fore, J. K. Sampson, S. Wachsmann-Hogiu, J. C. Rutledge, and T. Huser, Opt. Express **16**, 2168–2175 (2008).
[13] T. Hellerer, C. Axäng, C. Brackmann, P. Hillertz, M. Pilon, and A. Enejder, P. Natl. Acad. Sci. USA **104**, 14658 (2007).
[14] Y. M. Wu, H. C. Chen, W. T. Chang, J. W. Jhan, H. L. Lin, and I. Liau, Anal. Chem. **81**, 1496–1504 (2009).
[15] C. L. Evans, X. Xu, S. Kesari, X. S. Xie, S. T. C. Wong, and G. S. Young, Opt. Express **15**, 12076–12087 (2007).
[16] T. B. Huff, Y. Shi, Y. Fu, H. Wang, and J. Cheng, IEEE J. Sel. Top. Quant. **14**, 4 (2008).
[17] H. A. Rinia, K. N. J. Burger, M. Bonn, and M. Müller, Biophys. J. **95**, 4908–4914 (2008).
[18] C. L. Evans, E. O. Potma, M. Puoris'haag, D. Côté, C. P. Lin, and X. S. Xie, P. Natl. Acad. Sci. USA **102**, 16807–16812 (2005).
[19] J. X. Cheng, Y. K. Jia, G. Zheng, and X. S. Xie, Biophys. J. **83**, 502–509 (2002).
[20] X. Nan, E. O. Potma, and X. S. Xie, Biophys. J. **91**, 728–735 (2006).
[21] J. Wu, H. Soderbergh, K. Karlsson, and A. Danielsson, Hepatology **23**, 359–365 (1996).
[22] J. Wu, S. L. Liu, J. L. Zhu, P. A. Norton, S. Nojiri, J. B. Hoek, and M. A. Zern, J. Biol. Chem. **275**, 22213–22219 (2000).
[23] Y. Zhang, S. K. Venugopal, S. He, P. Liu, J. Wu, and M. A. Zern, Cell. Signal. **19**, 2339–2350 (2007).
[24] D. A. Hyson, T. G. Paglieroni, T. Wun, and J. C. Rutledge, Clin. Appl. Thromb. Hem. **8**, 147 (2002).
[25] J. Chan, S. Fore, S. Wachsmann-Hogiu, T. Huser, and K. Fund, Laser Photonics Rev. **2**, 325–349 (2008).
[26] S. Martin and R. G. Parton, Nat. Rev. Mol. Cell Biol. **7**, 373–378 (2006).
[27] C. Krafft, L. Neudert, T. Simat, and R. Salzer, Spectrochim. Acta A Mol. Biomol. Spectrosc. **61**, 1529–1535 (2005).
[28] J. E. Davies, P. Hodge, F. D. Gunstone, and K. Lie, Chem. Phys. Lipids **15**, 48 (1975).
[29] J. W. Chan, D. Motton, J. C. Rutledge, N. L. Keim, T. Huser, and A. R. S. Usda, Anal. Chem. **77**, 5870–5876 (2005).
[30] Y. M. Weng, R. H. Weng, C. Y. Tzeng, and W. Chen, App. Spectrosc. **57**, 413–418 (2003).
[31] A. Pol, S. Martin, M. A. Fernandez, C. Ferguson, A. Carozzi, R. Luetterforst, C. Enrich, and R. G. Parton, Mol. Biol. Cell **15**, 99–110 (2004).
[32] R. Jahn and R. H. Scheller, Nat. Rev. Mol. Cell Biol. **7**, 631–643 (2006).
[33] P. Boström, L. Andersson, M. Rutberg, J. Perman, U. Lidberg, B. R. Johansson, J. Fernandez-Rodriguez, J. Ericson, T. Nilsson, and J. Borén, Nat. Cell Biol. **9**, 1286–1293 (2007).
[34] S. O. Olofsson, P. Boström, L. Andersson, M. Rutberg, J. Perman, and J. Borén, BBA-Mol. Cell Biol. Lipids **1791**, 448–458 (2009).
[35] Miyanari, Y., K. Atsuzawa, N. Usuda, K. Watashi, T. Hishiki, M. Zayas, R. Bartenschlager, T. Wakita, M. Hijikata, and K. Shimotohno, Nat. Cell Biol. **9**, 1089–1097 (2007).
[36] N. A. Ducharme and P. E. Bickel, Endocrinology **149**, 942 (2008).
[37] L. L. Listenberger, X. Han, S. E. Lewis, S. Cases, R. V. Farese, D. S. Ory, and J. E. Schaffer, P. Natl. Acad. Sci. USA **100**, 3077–3082 (2003).
[38] A. E. Feldstein, N. W. Werneburg, A. Canbay, M. E. Guicciardi, S. F. Bronk, R. Rydzewski, L. J. Burgart, and G. J. Gores, Hepatology **40**, 185–194 (2004).
[39] J. P. Kampf and A. M. Kleinfeld, Physiology **22**, 7 (2007).
[40] J. A. Hamilton and F. Kamp, Diabetes **48**, 2255–2269 (1999).
[41] K. Tauchi-Sato, S. Ozeki, T. Houjou, R. Taguchi, and T. Fujimoto, J. Biol. Chem. **277**, 44507–44512 (2002).
[42] D. L. Brasaemle, J. Lipid Res. **48**, 2547 (2007).
[43] I. R. Corbin, E. E. Furth, S. Pickup, E. S. Siegelman, and E. J. Delikatny, BBA-Mol. Cell Biol. Lipids **1791**, 757–763 (2009)

